

The shape of the W_2B_5 particles do not indicate a large shape anisotropy. The particles are approximately 2 microns in size and are homogeneously distributed through the $AlMgB_{14}$ matrix. A spinel phase was detected, the light grey phase as indicated in figure 6.3.9 b. Although not indicated on the diagram the epoxy used when mounting the sample for polishing is the darkest phase and is found throughout the polished surface on which EDS analysis was performed.

6.3.4: The Production of Dense $AlMgB_{14}$

Literature reports indicate that 100% dense $AlMgB_{14}$ can be produced at temperatures of 1400°C from powders prepared from the elemental starting components². The compacts prepared in sections 6.3.1 and 6.3.2 were all prepared at 1400°C and the density of all the materials were well below 100%, as reported in table 6.3.1.

Various strategies were employed to densify the material. The effect of particle size on elemental and pre-reacted powders as well as the effect of starting composition (presence of Al liquid phase), temperature and pushing force were investigated to establish a route to dense sintered compacts.

6.3.4.1: The Effect of Particle Size

The ductile nature of metals often limits their ability to be milled to fine particle sizes. Although a range of variables including various milling speeds, milling media to powder mass ratios and mass % stearic acid added as a surfactant were employed in this study, it was found that aluminium (100 μm particle size) and magnesium (100 μm particle size) when milled, in the planetary mill, on their own or together weld together forming powders that are not less than 50 μm in size.

Elemental powders of Al, Mg and B were milled together in a planetary mill for different times. The particle sizes of the powders milled for different times were determined using laser diffraction techniques, table 6.3.4 a.

Additionally Al, Mg and B powders were milled together for 2 hours, pressed into green compacts and reacted at 1400°C in an uniaxial hot-press to form $AlMgB_{14}$.

These compacts (post reaction) were then crushed by pestle and mortar and this powder, referred to as the pre-reacted powder, was then milled for various times in the planetary mill. Particle sizes of these powders were also determined by laser diffraction, table 6.3.4 b.

Green compacts of the elemental and pre-reacted powders were then hot-pressed at 1400°C in an uniaxial hot press and the densities and porosities of the sintered compacts were determined using the Archimedes immersion method for density determination.

TABLE 6.3.4 a: Properties of elemental powders hot-pressed at 1400°C, 20 MPa, 1 hour

Milling Time (hours)	Particle size (μm)	Density (gcm^{-3})	Porosity (%)	Theoretical Density (gcm^{-3})
2	8.15	1.665	38.3	2.699
4	3.28	1.879	31.2	2.731
6	2.57	1.921	31.7	2.813
16	2.37	2.164	30.4	3.109

As the milling time increases the particle size of the elemental powder is reduced but the sintered compacts remain porous, $32.9 \pm 3.6\%$. The increase in the theoretical density of the compacts is due to the pickup of WC from the milling media. The presence of WC was identified from XRD due to W_2B_5 which become more pronounced in samples milled for greater than 4 hours.

TABLE 6.3.4 b: Properties of pre-reacted powders hot-pressed at 1400°C, 20 MPa, 1 hour

Milling Time (hours)	Particle size (μm)	Density (gcm^{-3})	Porosity (%)	Theoretical Density (gcm^{-3})
2	7.35	2.154	27.0	2.949
4	2.87	2.366	20.7	2.983
6	2.11	2.650	25.4	3.554
16	1.55	3.143	24.6	4.167

The brittle nature of AlMgB_{14} correlates with the particle size of the pre-reacted powder which is consistently smaller than the size of elemental powders obtained for the same milling time. The compacts produced from the pre-reacted powders are porous and the theoretical density is larger for the pre-reacted compacts than for the elemental compacts at all milling times due to the pickup of WC during the milling cycle.

As the milling time is increased, for both elemental powders and pre-reacted powders, the particle size decreases. The porosities of all the compacts hot-pressed at 1400°C are above 20%. Thus, dense compacts are not produced in the uniaxial hot-press at 1400°C for a load of 20 MPa for compacts prepared from smaller particle sized starting powders. Because of the intrinsic hardness of AlMgB_{14} , wear of the milling vessel is expected to be larger for the pre-reacted powders than for the elemental powders. The X-ray diffractograms for all of the pre-reacted compacts indicated the presence of W_2B_5 . ICP analysis was done on the pre-reacted composites and the results are presented in figure 6.3.10.

The amount of tungsten introduced into the starting powders increases as the milling time is increased. Based on the observed intensities in the XRD's for the various powders the amount of W is larger in pre-reacted powders than for elemental powders. This is so because the ratio of the peak heights of $\text{W}_2\text{B}_5:\text{AlMgB}_{14}$ is larger for pre-reacted powders than for elemental powders, figure 6.3.11.

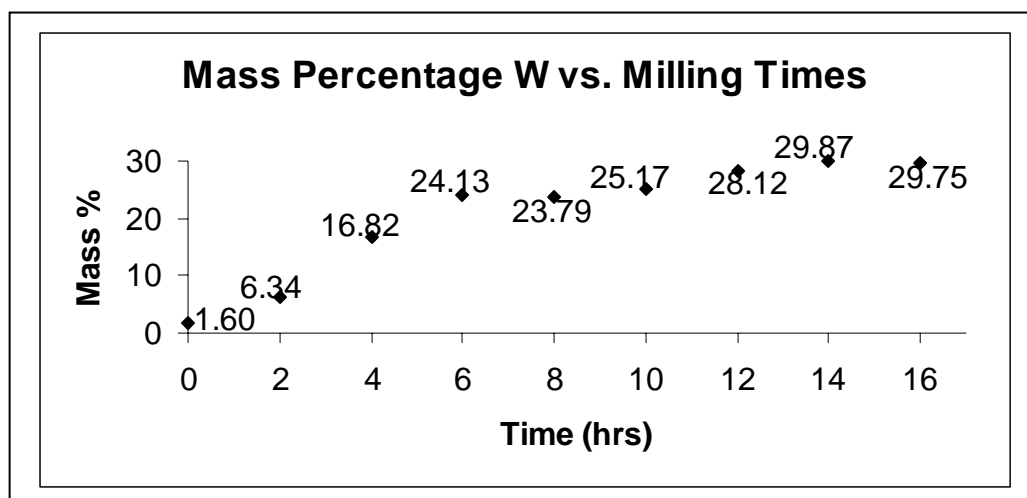


Figure 6.3.10: Mass percent of tungsten versus milling time for pre-reacted powders

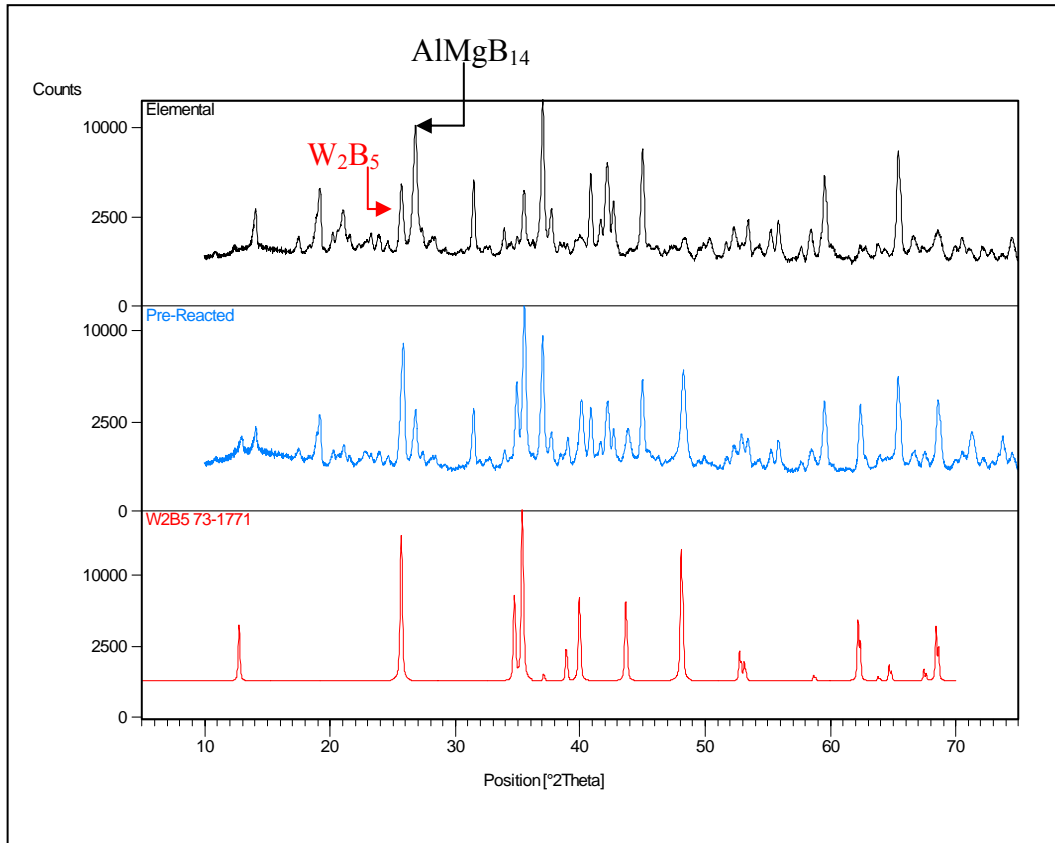


Figure 6.3.11: Comparison of elemental and pre-reacted AlMgB_{14} (6 hours milling) with W_2B_5

6.3.4.2: The Effect of Composition

The presence of a liquid phase during sintering is very beneficial for densification. This arises since the liquid phase facilitates mass transport thus enhancing the kinetics of the sintering process. Also, infiltration of the liquid phase into pores further densifies the material.

Aluminium and magnesium liquefy at 660 and 649°C respectively. Thus, in principle both metals would be suitable to form a liquid phase. However, magnesium boils at 1090°C which means that any unreacted magnesium would simply volatilise at the usual sintering temperature of 1400°C. Therefore, dependant on the phase diagram, magnesium is not a suitable liquid phase to facilitate densification at the sintering temperatures. Aluminium metal boils at 2467°C. Thus the excess liquid phase will exist through the entire duration of the sintering cycle as was shown in chapter 4.

Various amounts of each metal (values in wt.%) were added in excess to the starting powders and then sintered at 1400°C. The values for the compacts are reported in table 6.3.5.

TABLE 6.3.5: The densities, porosities and theoretical densities for elemental AlMgB₁₄ prepared with excess magnesium and/or aluminium and hot pressed at 1400°C, 20 MPa and 1 hour

Composition	Density (gcm⁻³)	Open Porosity (%)	Theoretical Density (gcm⁻³)
AlMgB ₁₄	1.696	36.0	2.649
+ 10 wt.% Mg	1.792	31.8	2.627
+ 10 wt.% Al	1.913	27.7	2.647
+ 10 wt.% (Al+ Mg)	1.829	31.6	2.675

The addition of excess aluminium increases the density of the sintered compact by 13% which is larger than the increase caused by addition of the magnesium metal which only increased the density by 6%. The larger increase in the density for the compact sintered with additional aluminium is expected since free Mg metal would volatilise at temperatures above its boiling point.

The addition of 10 wt.% of a 1:1 mole ratio excess of Al and Mg produces a sintered compact whose density is 8% denser than the sintered compact without any excess metal added. The compacts produced at 1400°C with excess metal added as a liquid phase during sintering produces compacts that are at best 28% porous for the aluminium addition.

The composition of the compacts can also be tailored so as to maximise the amount of AlMgB₁₄ present in the final sintered compact. As will be discussed in more detail in chapter 5, the formation of the spinel phase is largely dependent on the amount of oxide phase present in the starting powders. Thus, compacts produced from a 1:1 mole ratio of Al and Mg result in sintered materials that are deficient in Al and Mg because of the formation of the spinel phase from the oxide phases present in the

starting elemental powders. Based on Rietveld analysis, that was presented in chapter 5, about 10 wt.% of the spinel phase is present in the final compact for a material produced from a 1:1:14 mole ratio of Al:Mg:B. Therefore, compensation for the loss of the metals, assuming 10 wt.% spinel formation can be offset by adding additional amounts of Al and Mg in order to preserve the 1:1:14 stoichiometry of AlMgB_{14} . A detailed description of the calculation of the ratio of Al and Mg to be added in order to preserve the stoichiometry of AlMgB_{14} can be found in the experimental chapter. The abbreviation “CS” will be used to designate the additional amounts of Al and Mg added to AlMgB_{14} . This terminology will indicate that the loss of Al and Mg due to the formation of the spinel has been compensated for in the synthesis. Figure 6.3.12 indicates the effect of the addition of Al and Mg to the starting composition in order to maximise the amount of AlMgB_{14} present in the final sintered compact.

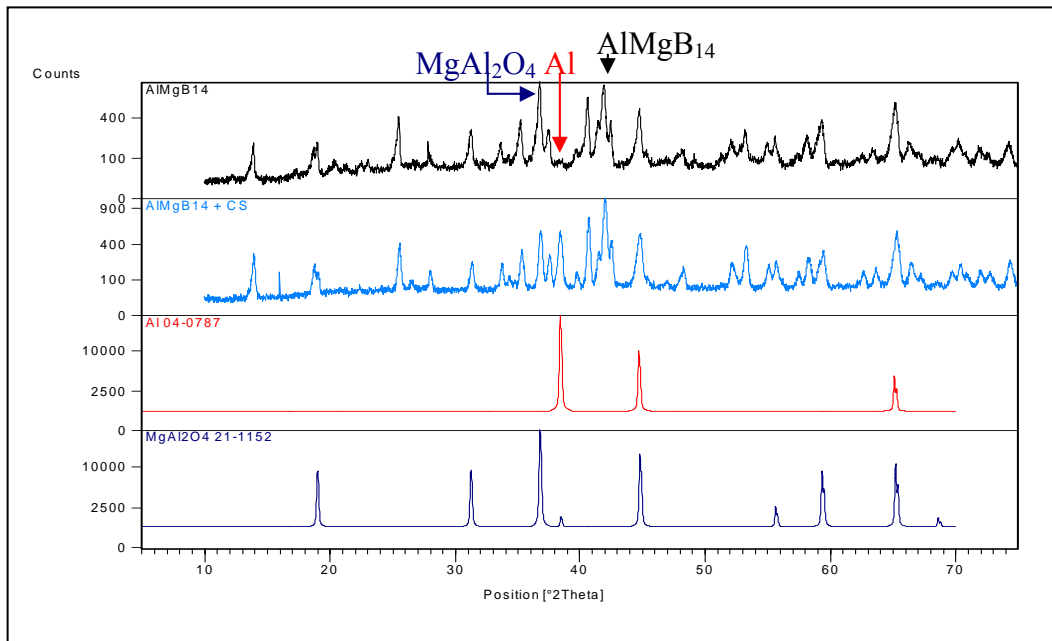


Figure 6.3.12: A comparison of AlMgB_{14} and $\text{AlMgB}_{14} +$ compensation for the spinel phase

Due to the change in the relative heights of the XRD peaks for MgAl_2O_4 and AlMgB_{14} it is clear from figure 6.3.12 that the addition of Al and Mg to compensate for the loss of these metals due to spinel formation, enhances the production of AlMgB_{14} . Additionally, there is free Al in the composite compensated for the spinel phase.

6.3.4.3: The Effect of Temperature

Elemental powders of Al, Mg and B (1:1:14 mole ratio) were milled for 2 hours in a planetary mill and pressed into green compacts and then hot-pressed at 900, 1000, 1200, 1400, 1500, 1600, 1700, 1800 and 1900°C (soak time 1 hour) at 20 MPa. Figure 6.3.13 a gives a summary of the diffractograms obtained for the samples prepared at 900, 1200, 1400, 1600 and 1700. Figure 6.3.13 b gives a detailed analysis of the XRD trace at 1600°C. Table 6.3.6 gives a summary of the densities, porosities of the sintered compacts and the ratio of the major XRD peak for AlMgB_{14} to the major XRD peak for MgAl_2O_4 .

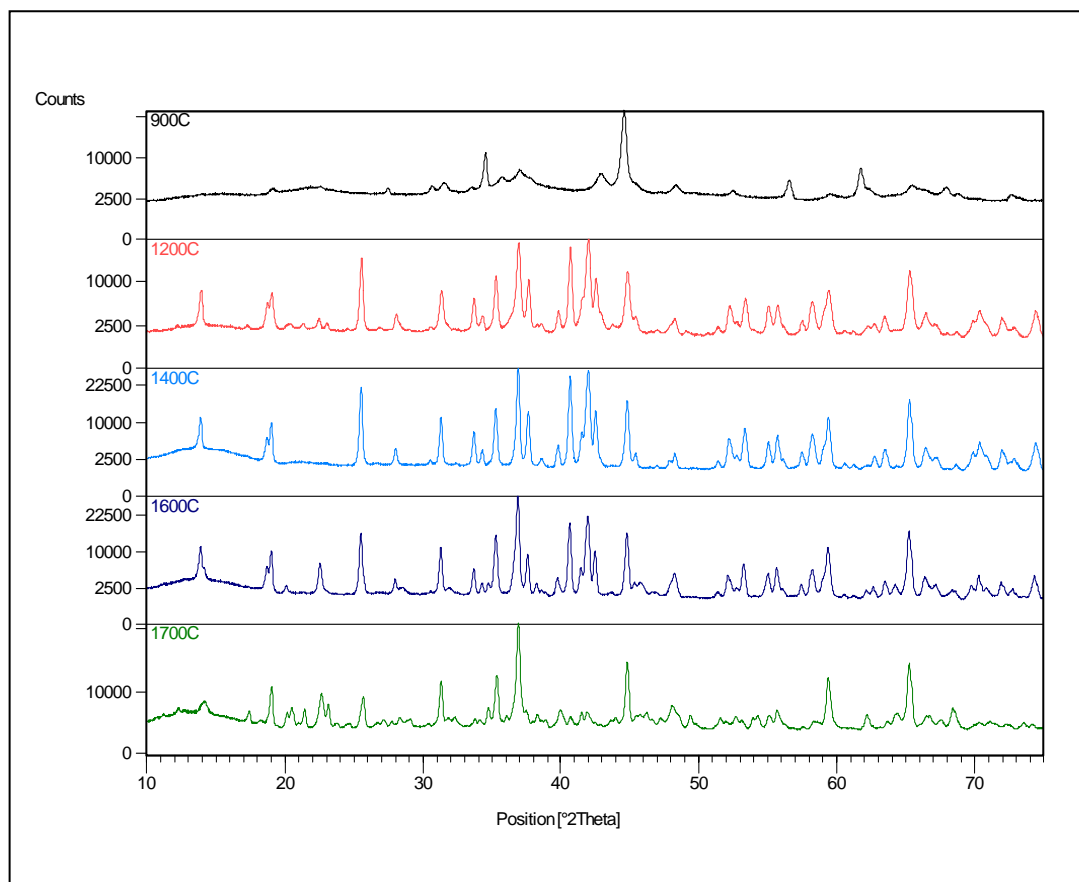


Figure 6.3.13 a: Comparison of the XRD patterns for AlMgB_{14} prepared at 900, 1200, 1400, 1600 and 1700°C

As can be seen from figure 6.3.13 a, AlMgB_{14} is not formed at temperatures of 900°C. The reasons for this are most likely kinetic because, as was addressed in detail in chapter 4, the formation of AlMgB_{14} is predicted at temperatures of 900°C. The spinel phase, MgAl_2O_4 and the boride phase AlMgB_{14} are both formed at temperatures of

1200°C and higher. The appearance of the peak at 23° 2θ belongs to carbon. The synthesis of this and all other composites take place in graphite dies. It is thus possible that carbon is found in the sample.

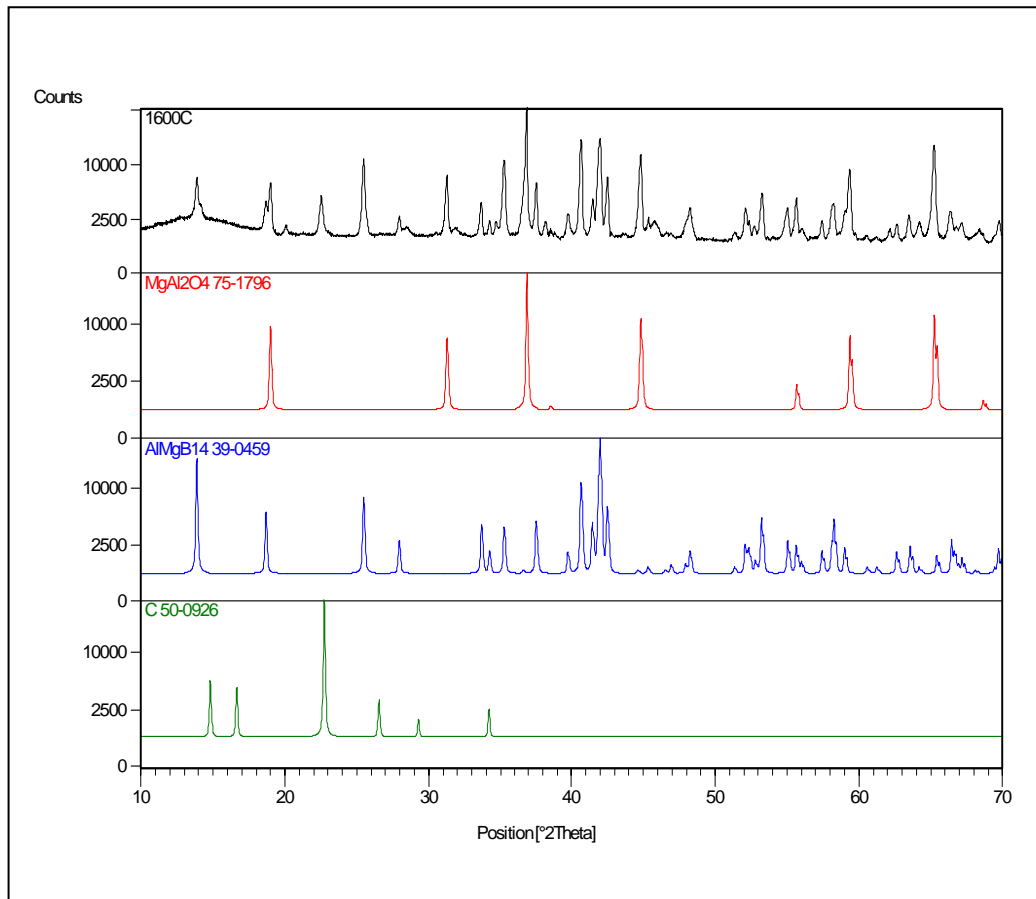


Figure 6.3.13 b: X-ray diffractogram for AlMgB₁₄ prepared at 1600°C

TABLE 6.3.6: Density, Relative Density and Porosity for AlMgB₁₄ prepared at 900°C, 1200°C, 1400 °C, 1500 °C, 1600 °C and 1700 °C

Temperature (°C)	Density (gcm ⁻³)	Relative Density (%)	Open Porosity (%)
900	1.313	48.9	51.1
1200	1.321	52.2	47.8
1400	1.665	62.6	38.3
1500	1.895	71.3	29.8
1600	2.111	79.4	21.1
1700	2.730	91.3	8.7

The decomposition of AlMgB₁₄ into γ -AlB₁₂ at temperatures above 1600°C is consistent with the literature which reports that AlMgB₁₄ decomposes into γ -AlB₁₂ at temperatures higher than 1550°C²⁶. From these experiments the optimum density for limited decomposition is achieved at 1600°C. Hence, subsequent samples were prepared at 1600°C.

The effect of pressure at a fixed temperature of 1600°C was then investigated in order to further attempt to densify the material.

6.3.4.4: The Effect of Pressure

Samples of molar composition AlMgB₁₄ were prepared at 1600°C in the hot-press and subjected to loads of 20 MPa and 75 MPa in the uniaxial hot-press. The results are presented in table 6.3.7. In addition to the densities and porosities for the samples prepared at the different loads the ratio of the major XRD peak for AlMgB₁₄ to MgAl₂O₄ is also given.

TABLE 6.3.7: The density, porosity and AlMgB₁₄:MgAl₂O₄ major peak ratio for samples prepared at 20 MPa and 75 MPa at 1600°C

Pressure (MPa)	Density (gcm⁻³)	Porosity (%)	Ratio $\frac{AlMgB_{14}}{MgAl_2O_4}$
20	2.111	21.1	3.30
75	2.631	< 1%	2.45

Porosity measurements determined from Archimedes densities are not accurate when samples contain only closed porosity. At a load of 75 MPa all the porosity in the compact is closed and an estimation of the exact porosity is given by image analysis of the polished microstructure, the value of which is shown in table 6.3.7.

6.3.4.5: Pre-Reacted Powder versus Elemental Powders

As detailed in section 6.3.3 and 6.3.4, 99% dense compacts are obtained from elemental powders that are sintered at 1600°C and 75 MPa in an uniaxial hot-press under a steady flow of argon gas. The driving force for sintering is larger for compacts in which a chemical reaction takes place. It is expected that compacts prepared from elemental powders should densify better than compacts prepared from pre-reacted powders. However, if the results from table 6.3.4 a and b are compared then compacts prepared from the pre-reacted powders produce denser compacts than compacts that are produced from the elemental powders. Table 6.3.8 summarises the comparative results.

TABLE 6.3.8: A comparison of the densities obtained from pre-reacted powders and elemental powders at 1400°C and 20 MPa

Milling Time (hrs)	Elemental (E) Relative Density (%)	Pre-Reacted (PR) Relative Density (%)	Open Porosity (%)	
			E	PR
2	61.7	73.0	38.3	27.0
4	68.8	79.3	31.2	20.7
6	68.3	74.6	31.7	25.4
16	69.6	75.4	30.4	24.6

A possible explanation for this is that because of the increased WC content for pre-reacted powders there will be more energy available for sintering as a result of the large $\Delta H = -702.5$ kJ/mol (calculated from Factsage, a thermodynamics software package) for the reaction $2WC + 13B \rightarrow 2B_4C + W_2B_5$. Although the formation of W_2B_5 occurs in compacts prepared from both the elemental powders and the pre-reacted powders the amount of W_2B_5 formed in the pre-reacted powders is larger and hence the driving force for sintering from the chemical reaction that forms W_2B_5 is larger in the pre-reacted powders.

Table 6.3.8 indicates the densities and porosities associated with compacts produced from elemental and pre-reacted powders at 1600°C at a pushing force of 75 MPa. Additionally, the compositions of both the elemental powders and pre-reacted powders have been varied as indicated in table 6.3.8.

Aluminium has been added in excess to facilitate mass transport. As was shown in chapter 4 a persistent Al liquid phase will be in equilibrium with $AlMgB_{14}$ at temperatures above 1400°C.

TABLE 6.3.8: Densities, porosities for elemental and pre-reacted powders prepared at 1600°C and 75 MPa

Composition (wt. %)	Elemental		Pre-Reacted	
	Density (gcm ⁻³)	‡Porosity (%)	Density (gcm ⁻³)	‡Porosity (%)
*A	2.411	6.2±1.1	2.677	1.0±0.2
*A + †CS	2.660	3.5±1.0	2.790	2.6±0.4
*A + †CS + 3 % Al	2.719	5.1±2.7	2.815	2.1±0.8
*A + †CS + 5% Al	2.691	4.3±1.1	2.795	2.4±0.4
*A + †CS + 10% Al	2.606	5.9±1.3	2.852	2.7±0.9

*A = composition AlMgB₁₄

† CS = compensation for spinel

‡Porosity = closed porosity

The porosities of the compacts were determined by pixel counting using an image analysis software package, the details of which are given in the experimental chapter. As was the case for compacts prepared at 1400°C the pre-reacted powders produce slightly denser compacts than the elemental compacts at 1600°C. This is expected due to the higher uptake of WC during the milling of pre-reacted powders. Dense compacts are produced for compacts prepared at 1600°C and 75 MPa from elemental and pre-reacted powders. Also, as the amount of aluminium metal is increased the amount of porosity does not seem to change significantly. Thus, the addition of more liquid phase has very little effect on the further removal of the closed porosity present in the compacts prepared from elemental and pre-reacted powders.

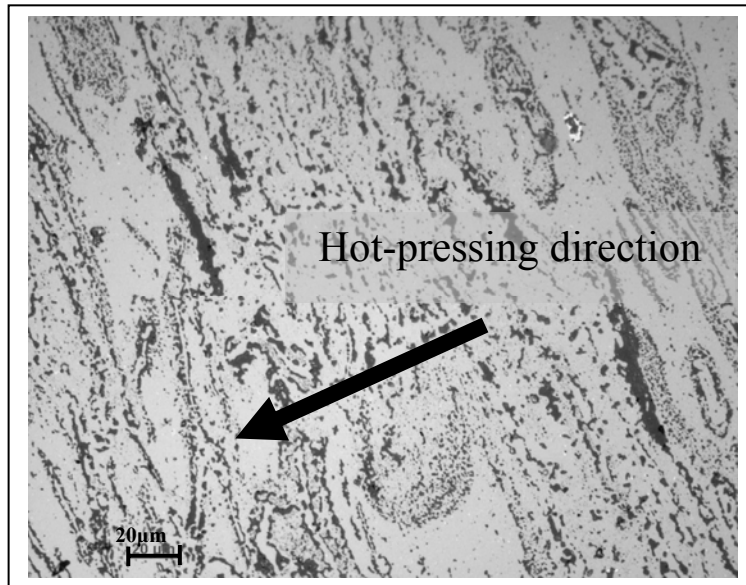


Figure 6.3.14 a: A microscope image taken for a compact produced from the elemental starting powder with composition A + CS + 3 wt.% Al at 1600°C and 75 MPa in an uniaxial hot-press

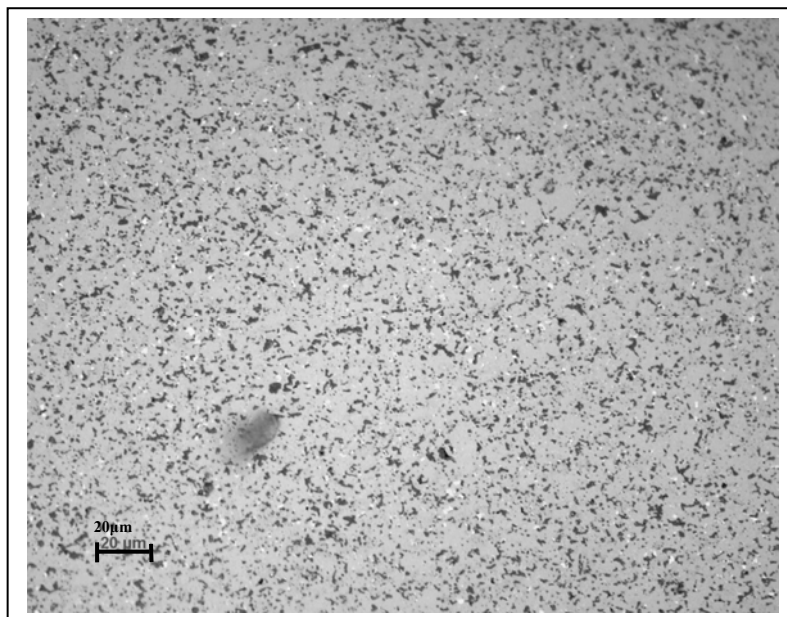


Figure 6.3.14 b: A microscope image taken at for a compact produced from the pre-reacted starting powder with composition A + CS + 3 wt.% Al at 1600°C and 75 MPa in an uniaxial hot-press

Figure 6.3.14 a and b present the microscope images of the elemental and pre-reacted powders with composition $\text{AlMgB}_{14} + \text{CS} + 3 \text{ wt.}\% \text{ Al}$ sintered in the uniaxial hot-press at 1600°C and 75 MPa. The different grey levels indicate that the microstructure formed for both composites are not homogeneous a more detailed analysis of the microstructure by SEM for the pre-reacted powder will be presented in section 3.3.5.2

It is important to note that there is a distinct preferential alignment direction in the compact prepared from the elemental powders. The direction of this alignment is perpendicular to the pressing direction. When comparing the images shown in figure 6.3.14 a and b, it is clear that the pre-reacted powders do not have any preferential alignment in the compact Thus, compacts produced from pre-reacted powders produce sintered compacts that have lower porosities than for the same compositions prepared from the elemental powders and the microstructures that do not have any structural anisotropy.

Based on this work the best synthesis procedure to produce dense AlMgB_{14} is to prepare pre-reacted AlMgB_{14} at 1400°C and 20 MPa. The mixture is then milled for a further 4 hours and the green compacts of this powder sintered at 1600°C and 75 MPa under argon gas in an uniaxial hot-press.

6.3.5: Microstructure and Mechanical Properties of compacts based on AlMgB_{14}

In this section of work the mechanical properties of AlMgB_{14} will be addressed. Specifically, the material's hardness and fracture toughness, measured as explained in chapter 2, will be presented. Because of the intrinsic hardness of AlMgB_{14} the uptake of WC from the milling vessel during the milling of pre-reacted AlMgB_{14} is inevitable. Thus, composites produced as detailed in section 6.3.4.3 and 6.3.4.5 will always contain WC. Hence, the composite discussed is actually $\text{AlMgB}_{14}\text{-WC}$. The presence of the spinel phase actually makes this material a composite of three phases; $\text{AlMgB}_{14}\text{-WC-MgAl}_2\text{O}_4$. For simplicity, this composite; $\text{AlMgB}_{14}\text{-WC-MgAl}_2\text{O}_4$ prior to sintering at 1600°C , will be referred to as the pre-reacted powder or PR.

6.3.5.1: The hardness of composites produced from pre-reacted AlMgB₁₄

The hardness of the PR compositions prepared in table 6.3.8 were evaluated on a Knoop hardness tester at a load of 500g. The results are presented in Table 6.3.9.

TABLE 6.3.9: The Knoop hardness of composites prepared in Table 6.3.8 at a 500 g load

Composition (wt. %)	Pre-Reacted		
	H _{K0.5} (GPa)	*Density (gcm ⁻³)	*Closed Porosity (%)
PR	19.9 ± 0.3	2.677	1.0±0.2
PR + CS	21.2 ± 0.8	2.790	2.6±0.4
PR + CS + 3wt. % Al	20.9 ± 0.7	2.815	2.1±0.8
PR + CS + 5wt. % Al	19.0 ± 0.8	2.795	2.4±0.4
PR + CS + 10wt. % Al	17.8 ± 1.1	2.852	2.7±0.9

*values presented in table 6.3.8

Because of the reduction in the amount of the spinel phase relative to AlMgB₁₄ by the compensation for the loss of Al and Mg and the slightly lower porosity and almost equivalent hardness to PR + CS, the composition PR + CS + 3wt. % Al (henceforth referred to as PR_{3CS}) was used to study the effect of various additives on the hardness and fracture toughness of the PR_{3CS} system. The choice of additive and the reasons for the choice will be discussed in each of the subsections to be presented. All samples up to now have been prepared at a 10°C/min heating rate and a 20°C/min cooling rate. It will be shown that samples prepared at heating rates of 100°C/min and cooling rates of approximately 100°C/min have a slightly lower porosity, higher hardness and fracture toughness for a PR_{3CS} + WC system. Thus, all samples presented in subsections 6.3.5.2-9 were prepared at heating rates and cooling rates of 100°C/min. The cooling rate is stated as approximate because at temperatures below 1000°C the heating rate is less than 100°C/min.

6.3.5.2: The PR_{3CS} system

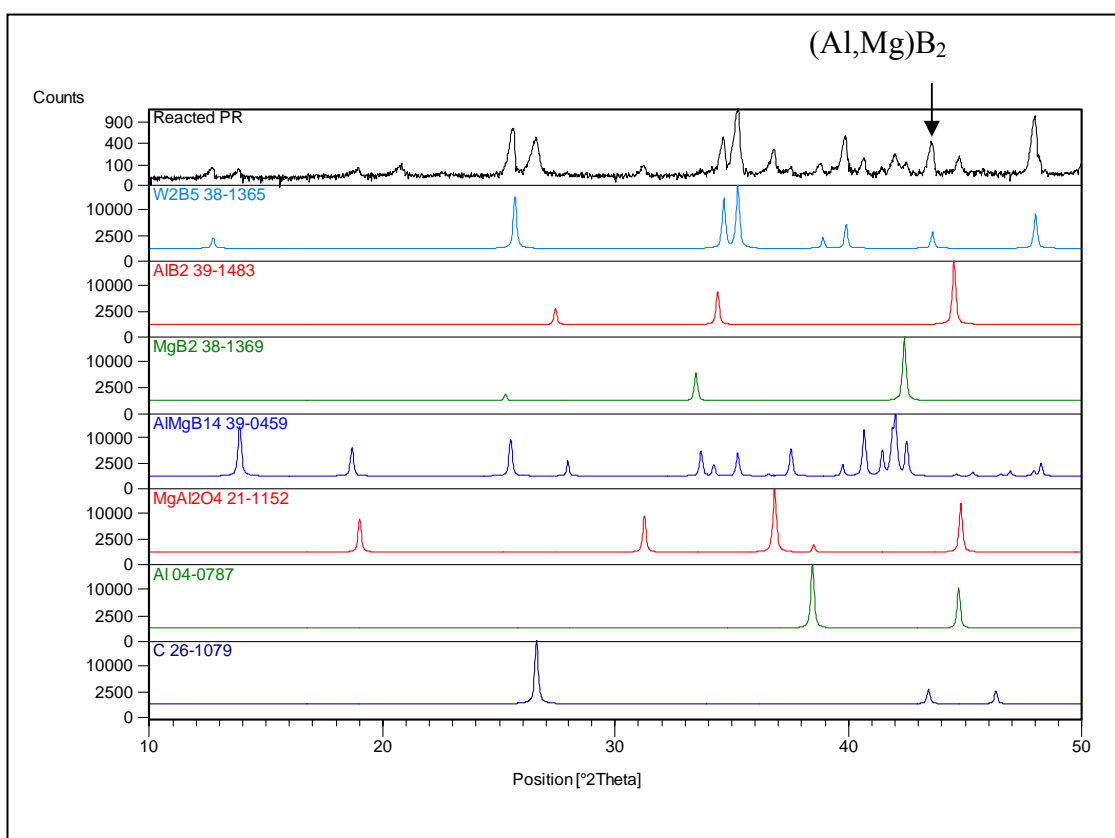


Figure 6.3.15a: Diffractogram for PR_{3CS} reacted at 1600°C, heating rate 100°C/min, soak time 1 hour, pressing force 75 MPa

The graphite pots in which all the samples have been prepared results in the presence of carbon, which has been identified by XRD analysis, to be present in all the samples. The presence of W₂B₅ dominates the diffractogram because of the high electron density associated with W. Thus, the presence of AlMgB₁₄ even when in large amounts, will present with smaller peak heights in the diffractogram.

The only source of boron in this sample is from AlMgB₁₄ and thus a reaction of WC with AlMgB₁₄ would yield three products W₂B₅, B₄C and (Al,Mg)B₂, equation 6.10. The presence of the (Al,Mg)B₂ phase is not clearly identified by XRD and neither is B₄C. As indicated in figure 6.3.15 a, the labelled peak may be due to the solid solution but because of the overlap with W₂B₅ it cannot be said with certainty that the solid solution phase is present. Additionally, if any solid solution phase is present in the sample the intensity of the peak will be very small. Free Al is not present in the

diffractogram for the reacted sample. This is more clearly illustrated in figure 6.3.15 b. The use of the words reacted and unreacted need to be clarified. Unreacted PR refers to the pre-reacted powder ($\text{PR}_{3\text{CS}}$) that has been prepared at 1400°C and milled for 4 hours. Reacted PR refers to the unreacted $\text{PR}_{3\text{CS}}$ subsequently hot-pressed at 1600°C , 1 hour soak time and 75 MPa. This convention will be adopted for all the composites presented forthwith.

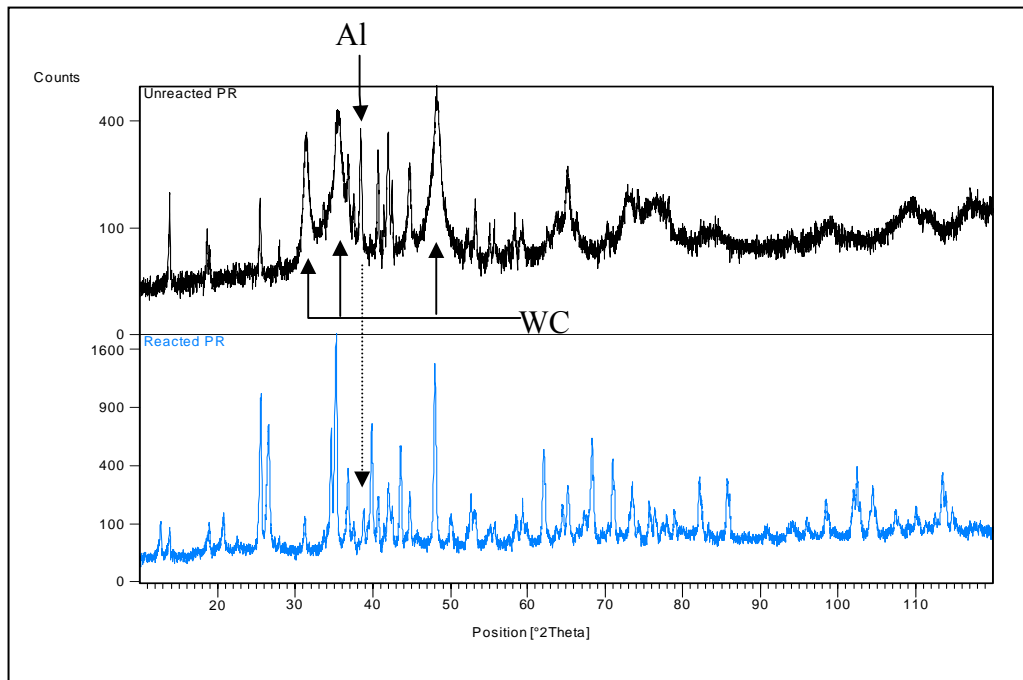


Figure 6.3.15 b: A comparison of unreacted $\text{PR}_{3\text{CS}}$ with reacted $\text{PR}_{3\text{CS}}$

It is important to note that the broad peaks (especially at higher angles) in the diffractogram for unreacted $\text{PR}_{3\text{CS}}$ is a result of the reduction in crystallite size of the WC that has been introduced during the milling cycle. The Al major peak is labelled in figure 6.3.15 b. Due to the change in the ratio of the peak height of the Al peak from the unreacted PR to the reacted PR, some of the excess Al must have reacted. It is not clear from the XRD what the excess Al has reacted with. An SEM micrograph is presented in figure 6.3.15 c. The major phases have been established from EDS analysis. The very bright platelets have been designated as W_2B_5 . Due to the sample processing route and sample preparation for SEM, carbon is detected by EDS throughout the material. EDS analysis confirmed that the platelets have less carbon in them than the more round shaped bright phase.

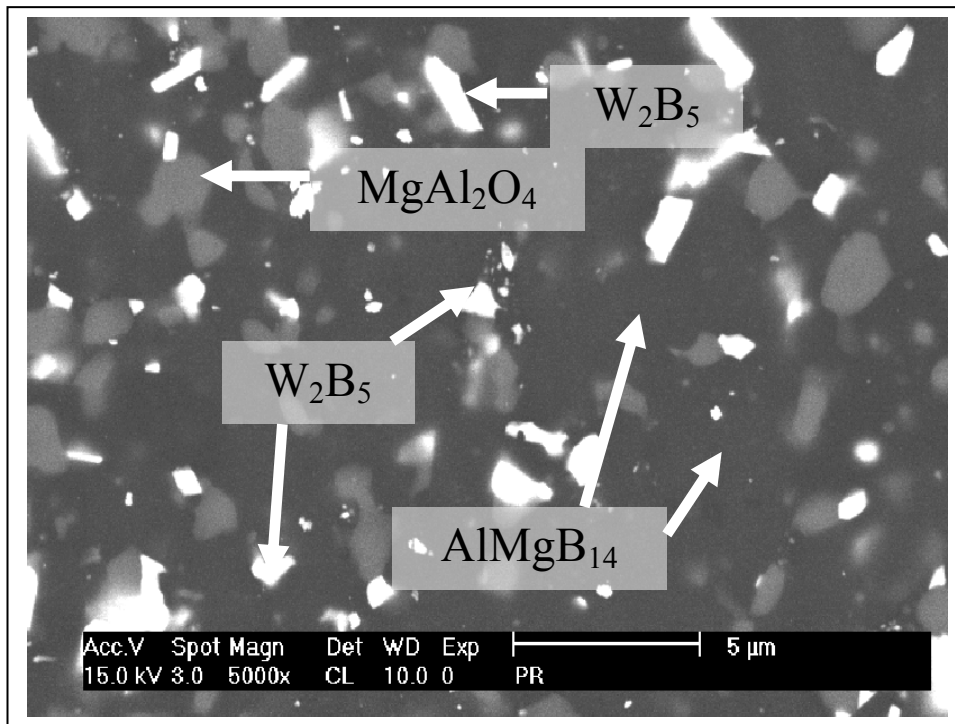


Figure 6.3.15 c: An SEM image for PR_{3CS}

6.3.5.3: PR_{3CS} + 30 wt.% TiB₂

Based on the results of Cook *et al*², 30 wt.% TiB₂ was added to the PR_{3CS} system. This addition was made after the PR_{3CS} had been synthesised at 1400°C and 20 MPa and crushed by pestle and mortar to a powder. This mixture, PR_{3CS} + 30 wt.% TiB₂ was then milled for a further 4 hours and then hot-pressed at 1600°C, soak time 1 hour, 75 MPa.

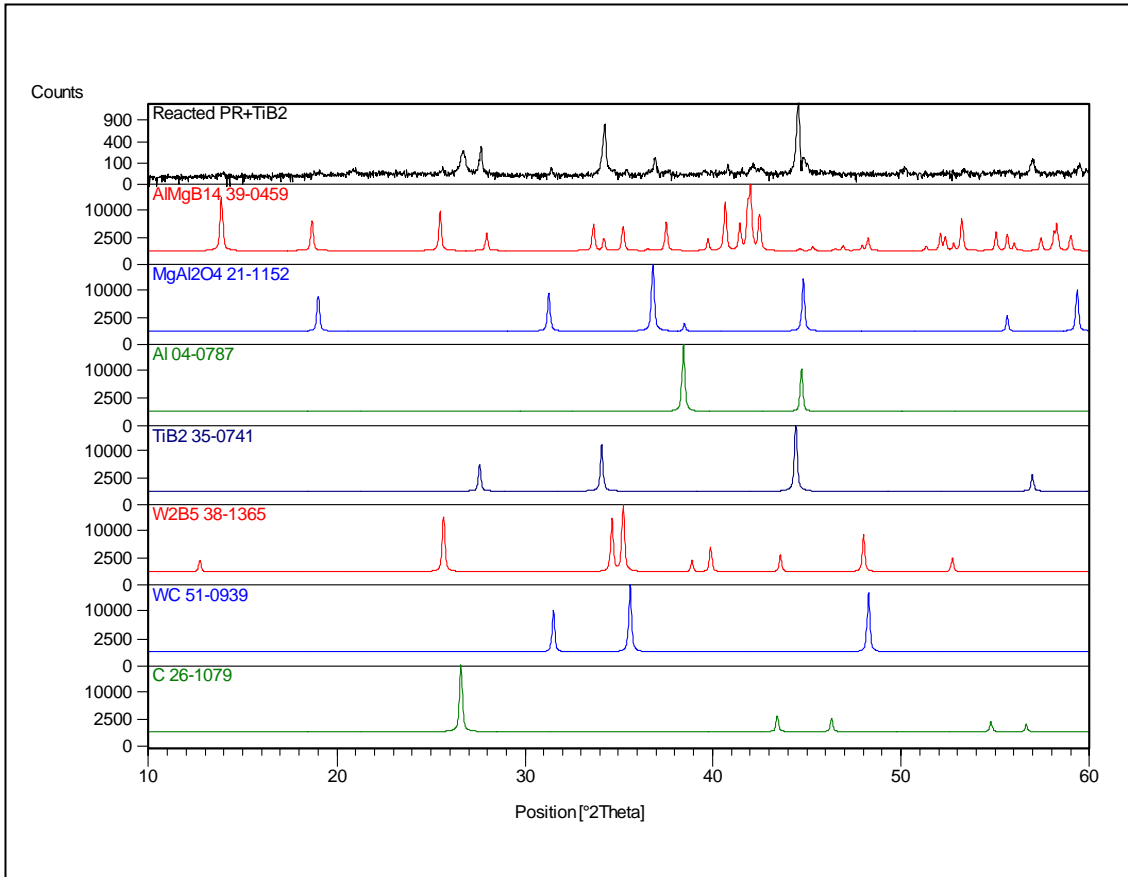


Figure 6.3.16 a: Diffractogram for $\text{PR}_{3\text{CS}} + 30 \text{ wt.}\% \text{ TiB}_2$ reacted at 1600°C , heating rate $100^\circ\text{C}/\text{min}$, soak time 1 hour, pressing force 75 MPa

The presence of 30 wt.% TiB_2 in the sample dominates the diffractogram. AlMgB_{14} is also present. The spinel is confirmed by XRD. W_2B_5 is not detected by XRD. Figure 6.3.16 b is a SEM image obtained in back scattered mode on a polished section of this material.

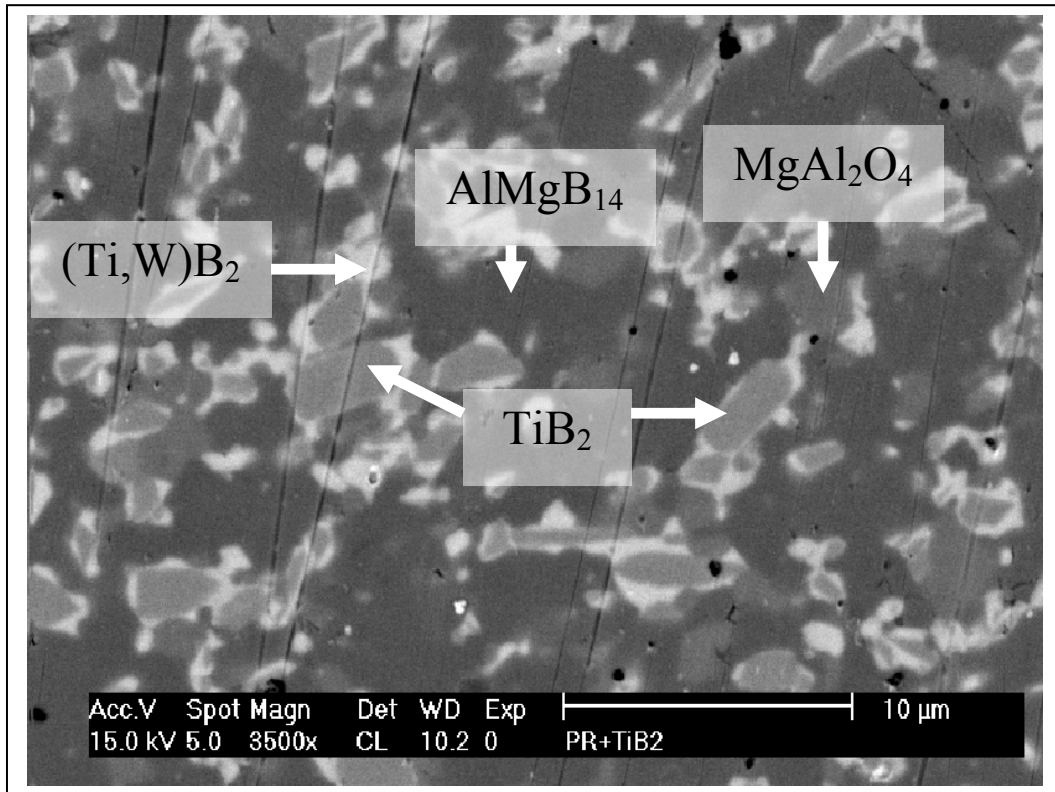


Figure 6.3.16 b: An SEM image for $\text{PR}_{3\text{CS}} + 30 \text{ wt.}\% \text{TiB}_2$

The TiB_2 phase (core) is surrounded by a brighter phase (rim). Both W_2B_5 and TiB_2 have hexagonal crystal systems. A solid solution phase, $(\text{Ti,W})\text{B}_2$, is therefore possible between these two phases. TiB_2 is a very stable solid and hence the diffusion of W into the TiB_2 grains is slow. Therefore, only the outer rim of the TiB_2 grains appears lighter as a result of the higher W content, which due to its higher electron density has a brighter contrast in back scattered mode in the SEM. As W_2B_5 dissolves into TiB_2 the W_2B_5 phase becomes less boron rich. Therefore, W_2B_5 adopts the stoichiometry of WB_2 , which also has hexagonal symmetry. The lattice parameters of TiB_2 (JCPDS 35-0741) and WB_2 (JCPDS 89-3928) are very similar. Thus, $(\text{Ti,W})\text{B}_2$ does not result in a pronounced shift in the TiB_2 XRD peaks. The bulk of the material is AlMgB_{14} and the spinel phase is slightly darker than the TiB_2 phase but brighter than the AlMgB_{14} phase.

6.3.5.4: PR₃CS + 5 wt.% Si

Based on the results of Cook *et al*², 5 wt.% Si was added in the same order as TiB₂ was added to the PR₃CS system.

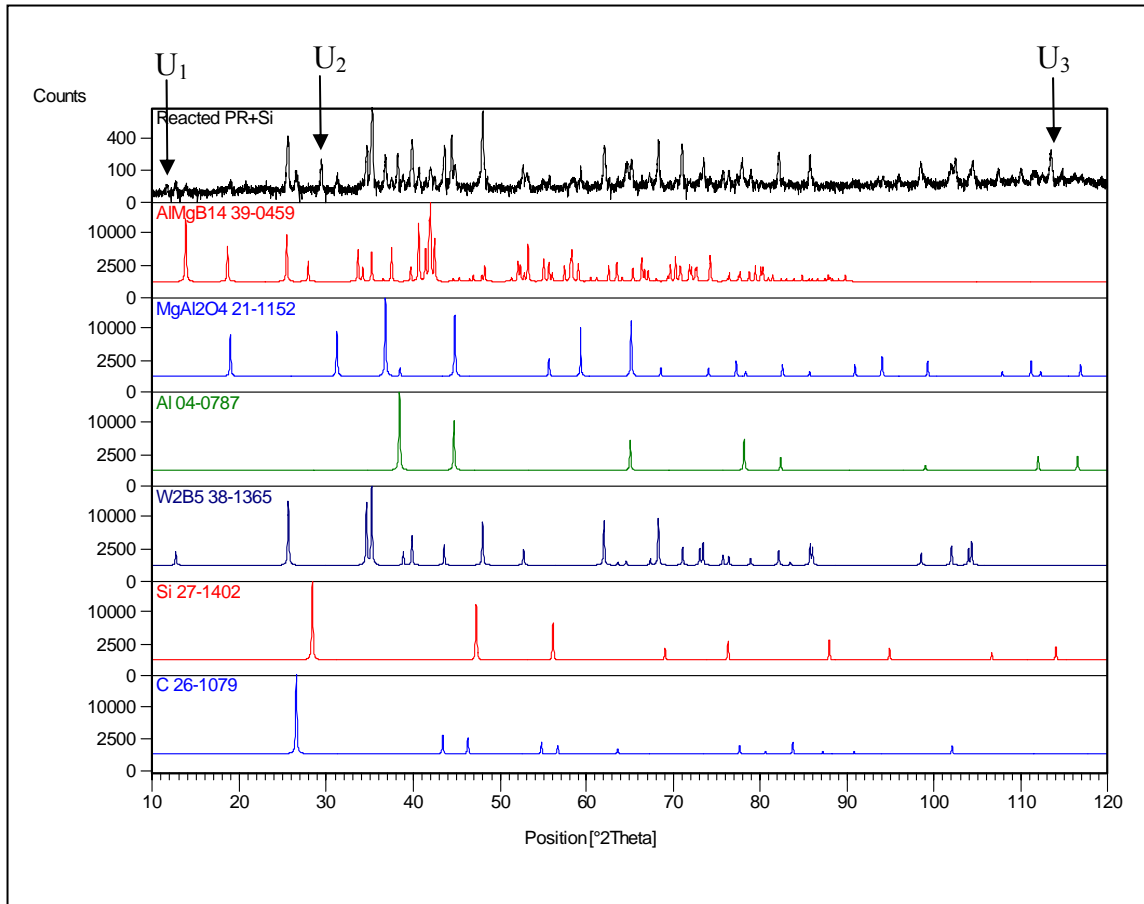


Figure 6.3.17 a: Diffractogram for PR₃CS + 5 wt.% Si reacted at 1600°C, heating rate 100°C/min, soak time 1 hour, pressing force 75 MPa

Al has been identified in this sample by XRD. Three unidentified peaks U₁, U₂ and U₃ were found. These peaks could be related to the formation of some additional SiB phases which could not be identified unequivocally from XRD. Further study of the phase content as a result of the formation of silicon borides would need to be done to fully understand what phases are formed in this composite. XRD evidence confirms that AlMgB₁₄ and MgAl₂O₄ and W₂B₅ are present in this sample. It is clear from figure 6.3.17 b that Si has reacted. Additionally, some of the Si could enter the AlMgB₁₄ structure as was has been proposed by Cook *et al*². No phases with a high Si content could be detected from XRD.

Figure 6.3.17 c is an image of the microstructure of a polished section of this sample in back scattered mode. W_2B_5 platelets can be seen in the microstructure.

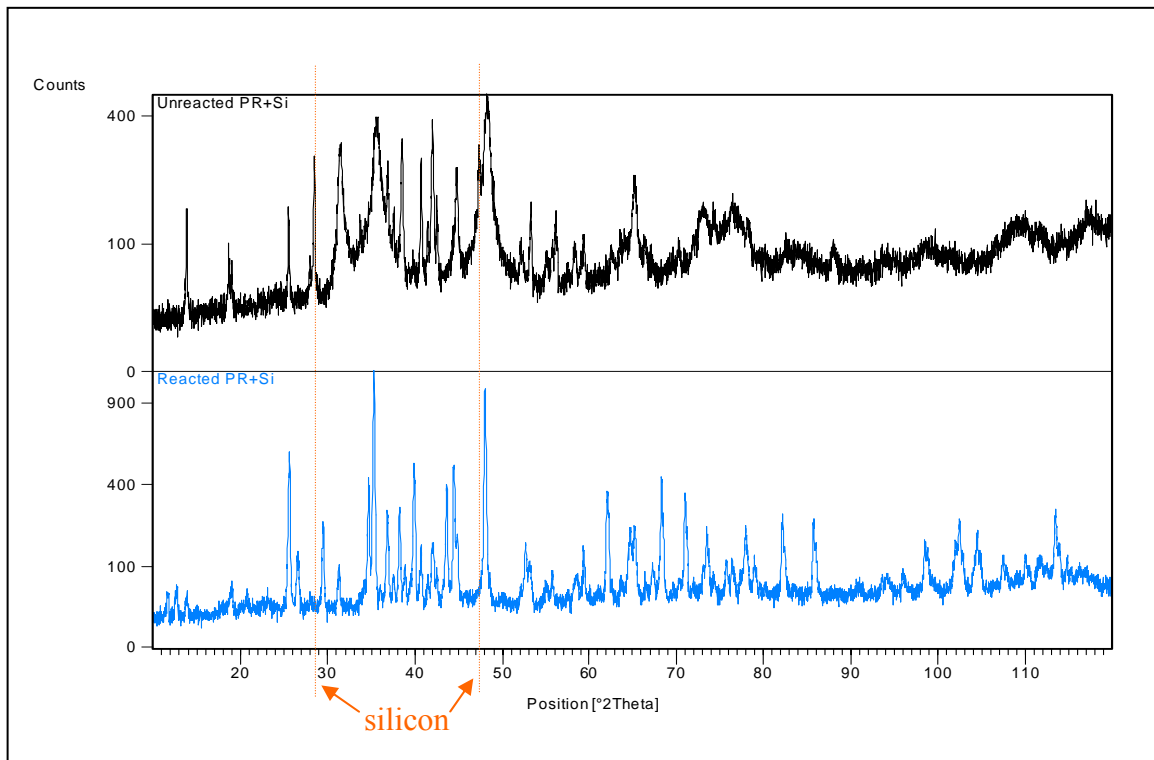


Figure 6.3.17 b: A comparison of unreacted $PR_{3CS} + 5 \text{ wt.}\% \text{ Si}$ with reacted $PR_{3CS} + 5 \text{ wt.}\% \text{ Si}$

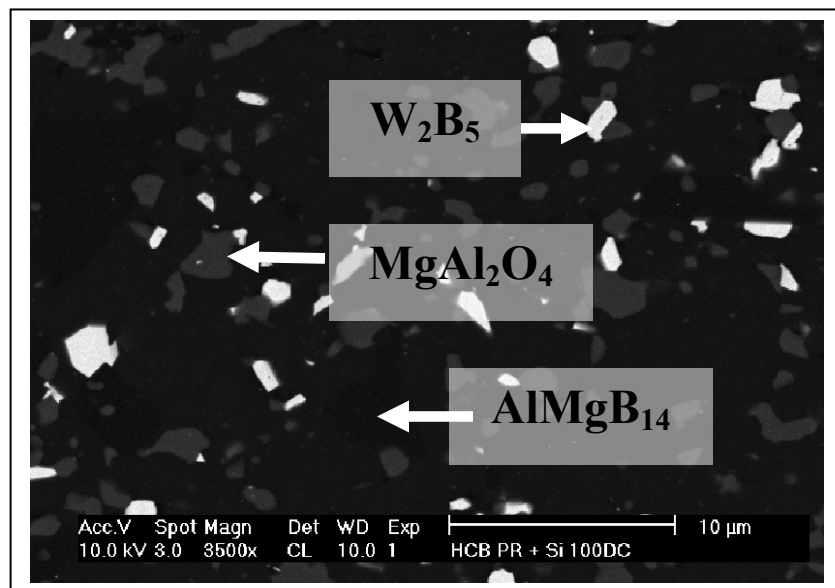


Figure 6.3.17 c: An SEM image for $PR_{3CS} + 5 \text{ wt.}\% \text{ Si}$

6.3.5.5: PR₃CS + 25.8 wt.% TiC

Cook *et al*² showed that the hardness of AlMgB₁₄ is improved by the addition of 30 wt.% TiB₂. It was shown in section 6.3.2.3 that TiC reacts with AlMgB₁₄ or B to yield TiB₂, reaction 6.3 and 6.4 respectively. Assuming a complete reaction of TiC with AlMgB₁₄, 25.8 wt.% TiC is required in order to produce a 30 wt.% TiB₂ composite with PR₃CS. To minimise the reaction of TiC with AlMgB₁₄ a second composite was made that contained additional boron (21.8 wt.%) so as to favour the reaction of TiC with B rather than with AlMgB₁₄. The results of the two composites PR₃CS + TiC and PR₃CS + TiC + B are presented. Figure 6.3.18 a is a diffractogram obtained for PR₃CS + TiC. Figure 6.3.18 b is a comparison of unreacted and reacted PR₃CS + TiC. Figure 6.3.18 c and d is a comparison of the diffractograms obtained for reacted PR₃CS + TiC and PR₃CS + TiC + B. Figure 6.3.18 e and f are SEM images of the microstructures obtained on polished sections of PR₃CS + TiC and PR₃CS + TiC + B.

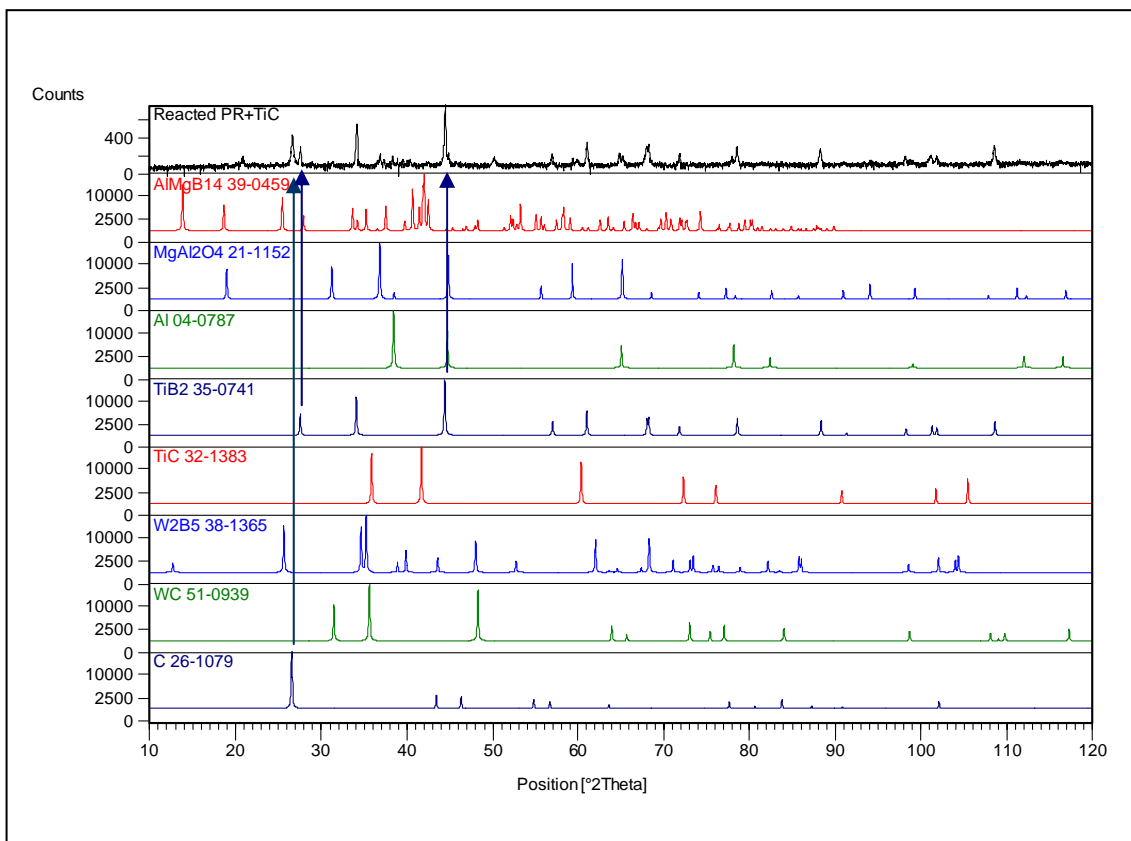


Figure 6.3.18 a: Diffractogram for PR₃CS + 25.8 wt.% TiC reacted at 1600°C, heating rate 100°C/min, soak time 1 hour, pressing force 75 MPa

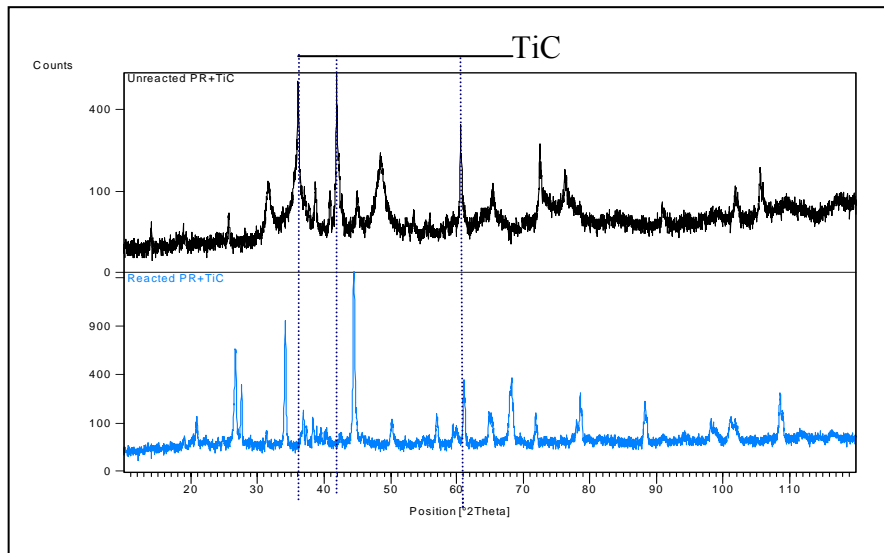


Figure 6.3.18 b: A comparison of unreacted $\text{PR}_{3\text{CS}}$ + 25.8 wt.% TiC with reacted $\text{PR}_{3\text{CS}}$ + 25.8 wt.% TiC

When figure 6.3.18 a is compared to figure 6.3.16 a it is clear that TiC reacts with AlMgB_{14} to form $(\text{Al,Mg})\text{B}_2$, TiB_2 and B_4C according to reaction 6.3. Because of the electron density associated with TiB_2 the less electron dense phases $[(\text{Al,Mg})\text{B}_2$ and $\text{B}_4\text{C}]$ are not clearly identified by XRD. Further evidence supporting the reaction of TiC with AlMgB_{14} is the disappearance of the TiC peaks in the reacted composite as highlighted in figure 6.3.18 b.

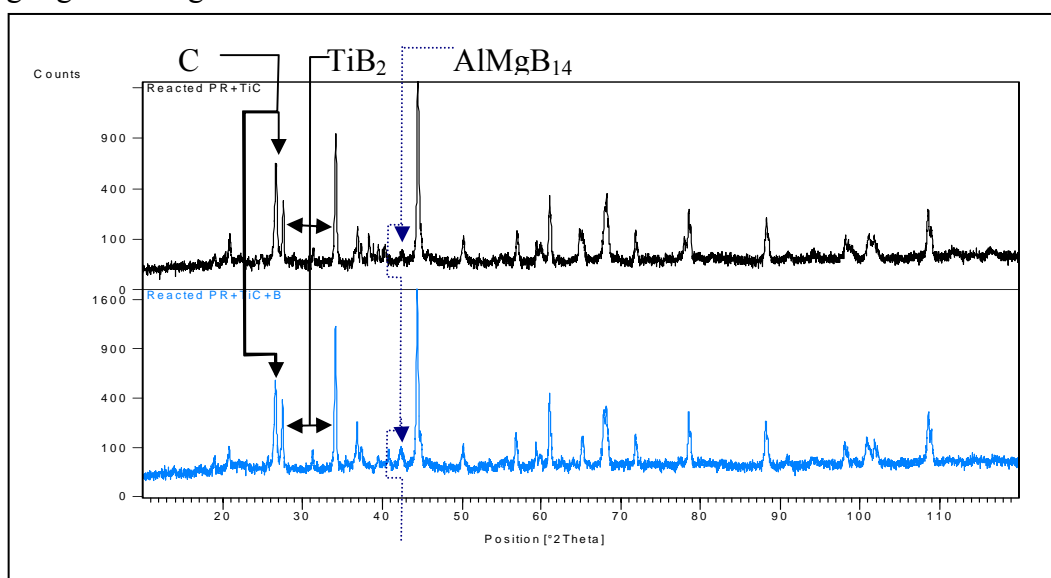


Figure 6.3.18 c: A comparison of reacted $\text{PR}_{3\text{CS}}$ + 25.8 wt.% TiC with reacted $\text{PR}_{3\text{CS}}$ + 25.8 wt.% TiC + 21.8 wt.% B